RESEARCH ARTICLE | DECEMBER 27 2022

High conductivity β-Ga_2O_3 formed by hot Si ion implantation

Arka Sardar ; Tamara Isaacs-Smith ; Jacob Lawson ; Thaddeus Asel; Ryan B. Comes ; Joseph N. Merrett ; Sarit Dhar

Appl. Phys. Lett. 121, 262101 (2022)
https://doi.org/10.1063/5.0127457

Applied Physics Letters ARTICLE scitation.org/journal/apl

High conductivity β-Ga_2O_3 formed by hot Si ion implantation

Cite as: Appl. Phys. Lett. **121**, 262101 (2022); doi: 10.1063/5.0127457
Submitted: 21 September 2022 · Accepted: 13 December 2022 ·
Published Online: 27 December 2022

Arka Sardar,[1,a] Tamara Isaacs-Smith,[1] Jacob Lawson,[2] Thaddeus Asel,[3] Ryan B. Comes,[1] Joseph N. Merrett,[3] and Sarit Dhar[1]

AFFILIATIONS

[1]Department of Physics, Auburn University, Auburn, Alabama 36849, USA
[2]University of Dayton Research Institute, Dayton, Ohio 45469, USA
[3]Air Force Research Laboratory, Wright-Patterson AFB, Ohio 45433, USA

[a)]Author to whom correspondence should be addressed: azs0222@auburn.edu

ABSTRACT

This work demonstrates the advantage of carrying out silicon ion (Si^+) implantation at high temperatures for forming controlled heavily doped regions in gallium oxide. Room temperature (RT, 25 °C) and high temperature (HT, 600 °C) Si implants were carried out into MBE grown (010) β-Ga_2O_3 films to form ~350 nm deep Si-doped layers with average concentrations up to $\sim 1.2 \times 10^{20}$ cm^{-3}. For such high concentrations, the RT sample was too resistive for measurement, but the HT samples had 82.1% Si dopant activation efficiency with a high sheet electron concentration of 3.3×10^{15} cm^{-2} and an excellent mobility of 92.8 $cm^2/V{\cdot}s$ at room temperature. X-ray diffraction measurements indicate that HT implantation prevents the formation of other Ga_2O_3 phases and results in reduced structural defects and lattice damage. These results are highly encouraging for achieving ultra-low resistance heavily doped Ga_2O_3 layers using ion implantation.

Ga_2O_3 is emerging as a promising wide bandgap semiconductor material and is attracting significant attention from the research community for power electronic applications.[1–3] Among different phases, the monoclinic β phase is thermally the most stable with a reported bandgap of 4.6–4.9 eV,[4] and a breakdown electric field of 8 MeV/cm,[5] which is much higher compared to SiC and GaN. β-Ga_2O_3 has robust chemical resistance and radiation hardness, which are attractive for devices operating in harsh environments.[5] In addition, the prospect of low-cost mass production due to a floating zone (FZ)[6] and an edge-defined film-fed (EFG)[6] growth method is also a key advantage for this material.

Ion implantation is attractive for device processing as it offers a way to selectively dope different regions of a material with precise control of dopant concentration and profile.[5] Sasaki *et al.*[7] performed Si implantation into β-Ga_2O_3 (010) at room temperature (RT) with concentrations ranging from 10^{19} to 10^{20} cm^{-3} followed by annealing ranging from 700 to 1100 °C. The highest carrier concentration and lowest resistivity were achieved for samples implanted with 5×10^{19} cm^{-3} and annealed at 1000 °C. The ratio of the free electron concentration to the total amount of Si in Ga_2O_3 (activation efficiency, η) was found to be 63% for 5×10^{19} cm^{-3} implant concentration. However, for a concentration of 10^{20} cm^{-3}, a severe drop in η to ~6% was reported, which resulted in a resistivity even higher than samples with the lowest implanted concentration of 1×10^{19} cm^{-3}. These experiments seemed to define a maximum effective implanted concentration of 5×10^{19} cm^{-3} for room temperature implanted Si into β-Ga_2O_3. In the case of 4H-SiC, high temperature (HT) Al^+ implantation results in a dramatic improvement in activation efficiency and conductivity over room temperature implantation due to lower defect densities and better recrystallization after annealing.[8] Also, improvement in electrical activation by high temperature ion implantation in Si is a well-established phenomenon.[9] In this work, it is demonstrated that ion implantation at elevated temperatures can be used to efficiently dope β-Ga_2O_3 as well.

To this end, 300 nm thick, unintentionally doped β-Ga_2O_3 films are grown by molecular beam epitaxy (MBE) on top of the Fe doped semi-insulating substrate using the process described in the supplementary material. Based on previous MBE runs, the doping and mobility of the film are estimated to be $\sim 2 \times 10^{16}$ cm^{-3} and 100 $cm^2/V{\cdot}s$, respectively, giving an approximate sheet resistance of 1×10^5 Ω/□. Samples were implanted with 275 and 425 keV Si^+ ions targeting a box profile approximately 300 nm thick as shown in the SRIM profile in Fig. 1. The SRIM[10] simulated profile for Si is shown in Fig. 1 that gave idea about two energies of implantation based on the

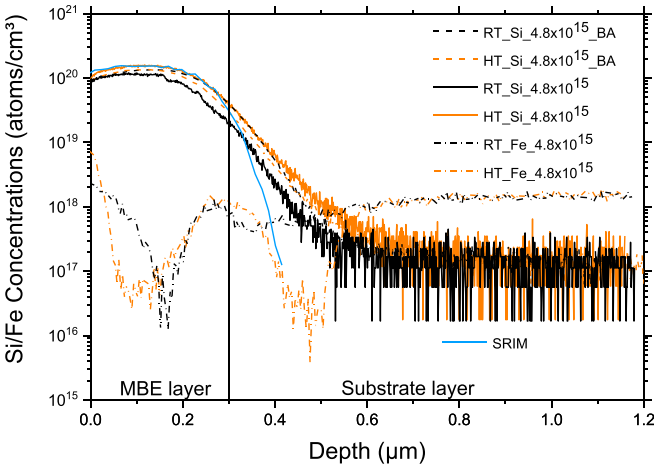

FIG. 1. SIMS profiles of Si^+ in β-Ga_2O_3 implanted with 275 and 425 keV Si^+ ions with a total fluence of $4.8 \times 10^{15}\,cm^{-2}$ for RT and HT implanted samples before and after annealing. The Si SRIM simulated profile and SIMS of Fe after annealing for RT and HT implanted samples are also shown.

targeted implant profile. The ion flux for the lower and higher energy was 4.61×10^{11} and 6.46×10^{11} ions/cm^2/s, respectively, maintaining identical beam current (1 μA for both energies with a chamber pressure of 3.0×10^{-6} Torr) for all the implants with total fluences of 2.4×10^{15} or $4.8 \times 10^{15}\,cm^{-2}$. To overcome the limitation of the lowest available Si^+ beam energy in the pelletron accelerator that was used (the lowest possible energy is ~100 KeV), 110 nm of Mo was used as an energy reducing layer to enable doping of the film with the target SRIM profile. A 30 nm thick Al_2O_3 layer was used between Mo and β-Ga_2O_3 to prevent any Mo knock-ons into β-Ga_2O_3. However, Al atoms get recoiled into the MBE film. Based on SRIM simulation (see supplementary material Fig. S1), this Al containing surface layer is ~15 nm and likely to be thinner due to wet etching of Al_2O_3 prior to annealing. Therefore, this layer is not likely to significantly impact the bulk electron transport results of the much thicker Si doped region. The implants were done with the sample holder at 21.6 °C (RT implants) and at 600 °C (HT implants). The temperature was measured at the back of the sample holder using a thermocouple as shown in Fig S4 of the supplementary material. After implantation, Mo and Al_2O_3 were removed by etching in hydrogen peroxide and a commercial (1:7) buffered oxide etch, respectively. This was followed by annealing in flowing nitrogen at 970 °C for 30 min to anneal the implant damage and activate the dopants. Optical and atomic force microscopy was performed after implantation and annealing. The RMS roughness (R_q) was less than 1 nm for all samples. However, the higher fluence RT sample had long (~mm) line-like features throughout the surface after annealing possibly due to surface reconstruction (see AFM and optical micrographs in the supplementary material) that require further investigation.

Secondary ion mass spectrometry (SIMS) profiles of Si in samples implanted with a fluence of $4.8 \times 10^{15}\,cm^{-2}$ at HT and RT before and after activation annealing are shown in Fig. 1. The SIMS profiles are deeper than the simulated profile possibly due to partial channeling of the ions into the crystal lattice since the samples were not tilted during implantation. The RT implanted sample prior to annealing had similar Si ion distribution to that of the as implanted HT sample. After annealing, however, the Si concentration increased in HT whereas it decreased for RT. More measurements are required to determine the reason for this or whether it is a real effect. Previously, it has been reported that ion induced damage at the film/substrate interface results in enhanced out-diffusion of Fe from the substrate into the film.[11] This is observed here as well, but the Fe profiles are comparable for the RT and HT implantation after activation as shown in Fig. 1. The thickness of the conducting layer was considered as the depth at which the Si concentration falls to $10^{19}\,cm^{-3}$, where compensation effects of Fe would not affect the conductivity. The dip of the Fe profile in the MBE layer is likely due to the interplay between damage and diffusion[11] during annealing, but further investigation is needed for more evidence.

Hall measurement was performed in the van der Pauw configuration in the temperature range of 27–325 °C. The contacts were made by depositing Ti/Au at four corners of the nominally square sample followed by annealing in an argon (Ar) atmosphere at 550 °C for 5 min. Multiple measurements were made, and the average values are reported here with the error bars representing the standard deviation of the measurements. Figure 2 shows that the sample implanted at high temperatures with the higher fluence has the lowest sheet resistance of 20.8 ± 0.68 Ω/□ at 27 °C. On the other hand, the higher fluence RT implanted sample was too resistive for measurement. For the lower fluence, the HT and RT samples had sheet resistances of 41.4 ± 8.24 and 51.3 ± 1.4, respectively, at 27 °C. At higher temperature, the overall resistance increased for all samples, but the HT implanted samples maintained advantage even at 325 °C.

The average sheet electron concentrations (n_s) are shown in Fig. 3. In Table I, the activation efficiencies η for all the samples are listed. Here, η was determined as the ratio of n_s and the total amount of Si obtained by integrating the SIMS profiles. For the lower fluence, RT and HT implanted samples, η are equal to about 68.2% and 76.3%,

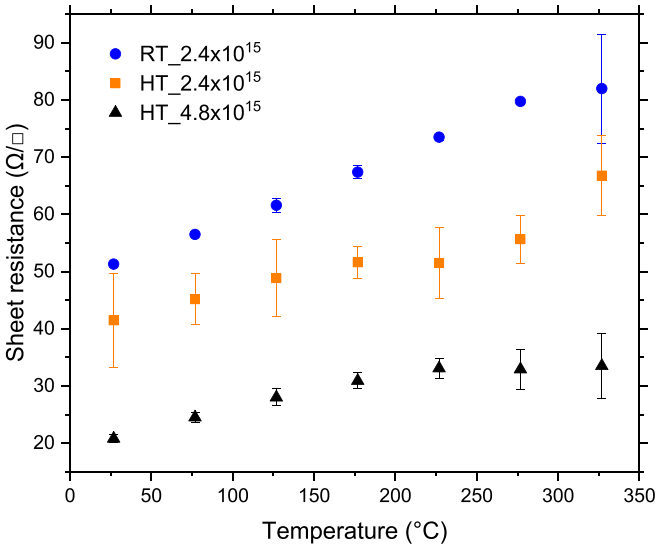

FIG. 2. Sheet resistance vs temperature for samples implanted at HT and RT with total Si^+ fluences of 2.4×10^{15} and $4.8 \times 10^{15}\,cm^{-2}$. Error bars represent variations over four measurements.

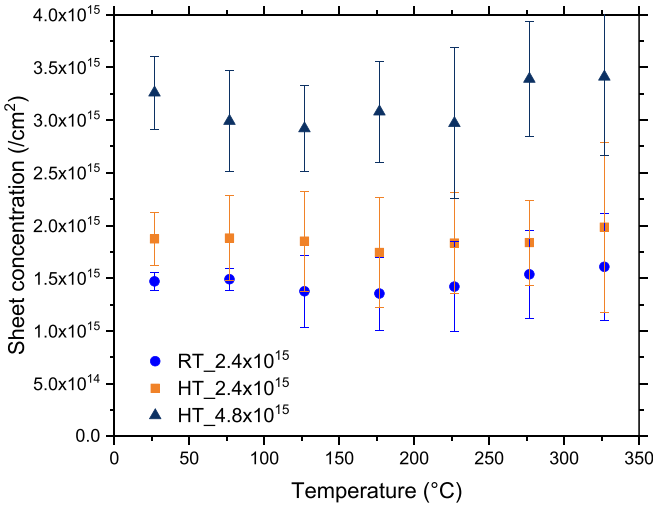

FIG. 3. Sheet charge concentration vs temperature for samples implanted at HT and RT with total Si^+ fluences of 2.4×10^{15} and $4.8 \times 10^{15}\,cm^{-2}$. Error bars represent variations over four measurements.

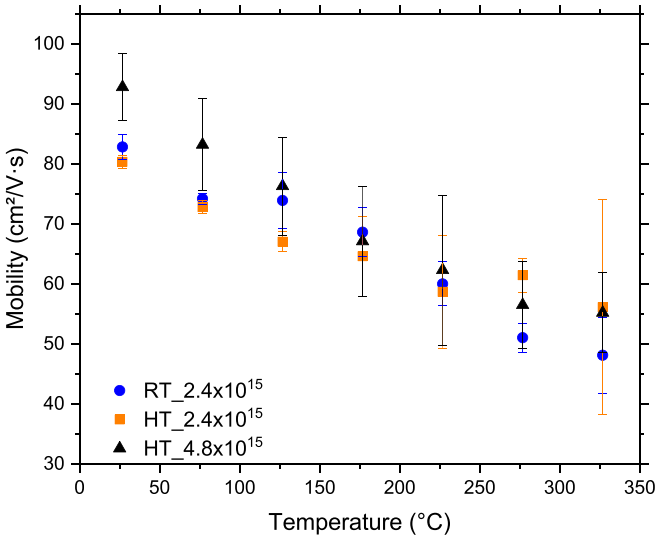

FIG. 4. Electron mobility vs temperature for HT and RT implanted samples' total fluences of Si^+ ions of 2.4×10^{15} and $4.8 \times 10^{15}\,cm^{-2}$. Error bars represent variation over four measurements.

TABLE I. Activation efficiency (η) comparison.

Nominal fluence ($/cm^2$)	Implantation temperature	Activation efficiency (η) (%)
2.4×10^{15}	RT (27 °C)	68.2
2.4×10^{15}	HT (600 °C)	76.3
4.8×10^{15}	RT (27 °C)	~0
4.8×10^{15}	HT (600 °C)	82.1

respectively, a modest advantage in favor of the HT sample. Remarkably, for the higher fluence HT sample, η is ~82.1%, which results in the increased electron sheet concentration. The likely reason for maintaining the high η is the reduction of ion induced compensating defects such as vacancies, interstitials, and/or their complexes by high temperature implantation. Figure 4 shows the electron Hall mobility as a function of temperature. For the lower fluence, mobility of HT and RT samples are 80.2 ± 1.1 and $82.8 \pm 2.14\,cm^2/V{\cdot}s$, respectively, at 27 °C. For the higher fluence, the mobility increases to $92.8 \pm 5.64\,cm^2/V{\cdot}s$ (at 27 °C). This unusual trend of increasing mobility with higher electron concentration could be due to enhanced screening of the electron phonon-scattering by the increased carrier density[12] and requires further investigation.

To study the crystal quality and strain, x-ray diffraction was performed using a Rigaku SmartLab XRD system using a Ge (220)×2 monochromator. Figure 5 shows HRXRD data for the higher fluence samples at the three different stages: as received, after Si implantation, and after activation annealing. The excellent crystal quality of the as received homoepitaxial samples is evident in the FWHM value of 52.5 arc sec corresponding to the (020) peak. After RT Si implantation

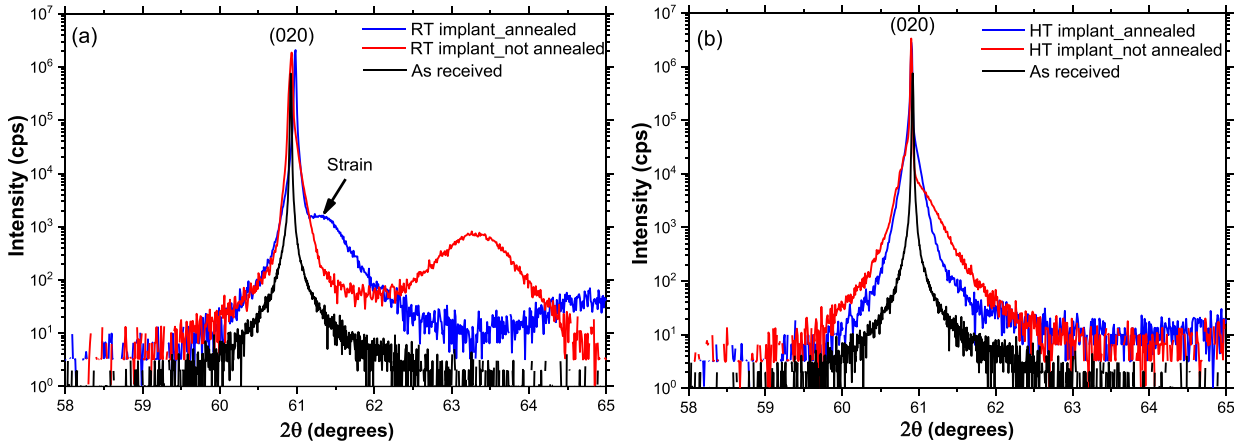

FIG. 5. HRXRD data for Ga_2O_3 implanted with $4.8 \times 10^{15}\,cm^{-2}$ Si^+ at (a) RT and (b) HT before and after annealing compared to the as-received MBE sample spectrum.

[red in Fig. 5(a)], the FWHM increased to 122 arc sec consistent with ion implantation induced defect creation and strain. An additional broader peak with a FWHM of 196.5 arc sec also appeared centered at 63.3°, which indicates the formation of a different phase; it is identified in the literature as κ-Ga_2O_3[13,14] or γ-Ga_2O_3.[15] On the other hand, no additional phase is observed for HT implantation [red in Fig. 5(b)], but broadening and distortion of the (020) peak is evident. After annealing at 970 °C, the broader peak in RT samples [blue in Fig. 5(a)] disappears, but an additional side shoulder appears at an angle higher than the original peak position along with a shift of the (020) peak, which can be attributed to the accretion of compressive strain in previous studies,[13,16–18] although due to the strong anisotropy of Ga_2O_3, it does not necessarily hold for other orientations. The strain peak is significantly smaller in the HT samples after annealing [blue in Fig. 5(b)]. However, the ion damage is not completely recovered, possibly due to the residual strain[19] suggesting optimization of the process is further needed. For the lower dose samples, similar effects were observed, and the results are included in the supplementary material.

In conclusion, we have demonstrated the advantage of HT ion implantation for forming heavily doped ($>10^{20}$ cm^{-3}) n-type regions in β-Ga_2O_3 devices and resistivity as low as 0.68 mΩ cm. Using Si^+ as the dopant, we observe a substantial increase in the sheet electron concentration and, consequently, a significantly lower sheet resistance compared to room temperature implantation. In addition, HRXRD shows that HT implantation causes reduced structural defects and strain in the implanted layer by preventing formation of any other phase. Being able to maintain the high mobility for carrier concentrations above 10^{20} cm^{-3} due to the impressive dopant activation efficiency makes it pertinent to further investigate the limits of high temperature ion implantation in β-Ga_2O_3.

See the supplementary material for the details of the MBE growth process, AFM, and XRD for lower fluence samples.

The authors thank Mr. Max Cichon, Accelerator Laboratory, Department of Physics, Auburn University for support with these experiments. HRXRD was performed with a Rigaku SmartLab instrument purchased with support from the National Science Foundation Major Research Instrumentation Program through Grant No. NSF-DMR-2018794. R.B.C. gratefully acknowledges funding from the Air Force Office of Scientific Research under Award No. FA9550-20-1-0034. EAG, Inc. provided SIMS services.

AUTHOR DECLARATIONS

Conflict of Interest

The authors have no conflicts to disclose.

Author Contributions

Arka Sardar: Investigation (equal); Writing – original draft (equal). **Tamara Isaacs-Smith:** Investigation (equal); Writing – review & editing (equal). **Jacob Lawson:** Investigation (equal); Writing – review & editing (equal). **Thaddeus J. Asel:** Investigation (equal); Writing – review & editing (equal). **Ryan Comes:** Investigation (equal); Writing – review & editing (equal). **Joseph Neil Merrett:** Conceptualization (equal); Resources (equal); Writing – review & editing (equal). **Sarit Dhar:** Investigation (equal); Writing – review & editing (equal).

DATA AVAILABILITY

The data that support the findings of this study are available from the corresponding author upon reasonable request.

REFERENCES

[1]M. Higashiwaki and G. H. Jessen, Appl. Phys. Lett. **112**, 060401 (2018).
[2]S. J. Pearton, J. Yang, P. H. Cary, F. Ren, J. Kim, M. J. Tadjer, and M. A. Mastro, Appl. Phys. Rev. **5**, 011301 (2018).
[3]A. J. Green, J. Speck, G. Xing, P. Moens, F. Allerstam, K. Gumaelius, T. Neyer, A. Arias-Purdue, V. Mehrotra, A. Kuramata, K. Sasaki, S. Watanabe, K. Koshi, J. Blevins, O. Bierwagen, S. Krishnamoorthy, K. Leedy, A. R. Arehart, A. T. Neal, S. Mou, S. A. Ringel, A. Kumar, A. Sharma, K. Ghosh, U. Singisetti, W. Li, K. Chabak, K. Liddy, A. Islam, S. Rajan, S. Graham, S. Choi, Z. Cheng, and M. Higashiwaki, APL Mater. **10**, 029201 (2022).
[4]M. J. Tadjer, J. L. Lyons, N. Nepal, J. A. Freitas, A. D. Koehler, and G. M. Foster, ECS J. Solid State Sci. Technol. **8**, Q3187 (2019).
[5]A. Nikolskaya, E. Okulich, D. Korolev, A. Stepanov, D. Nikolichev, A. Mikhaylov, D. Tetelbaum, A. Almaev, C. A. Bolzan, A. Buaczik, R. Giulian, P. L. Grande, A. Kumar, M. Kumar, and D. Gogova, J. Vacuum Sci. Technol. A **39**, 030802 (2021).
[6]H. Aida, K. Nishiguchi, H. Takeda, N. Aota, K. Sunakawa, and Y. Yaguchi, Jpn. J. Appl. Phys. **47**, 8506 (2008).
[7]K. Sasaki, M. Higashiwaki, A. Kuramata, T. Masui, and S. Yamakoshi, Appl. Phys. Express **6**, 086502 (2013).
[8]F. Roccaforte, F. Giannazzo, and G. Greco, Micro **2**, 23 (2022).
[9]G. A. Kachurin, I. E. Tyschenko, and L. I. Fedina, Nucl. Instrum. Methods Phys. Res. Sect. B: Beam Interact. Mater. Atoms **68**, 323 (1992).
[10]J. F. Ziegler, M. D. Ziegler, and J. P. Biersack, Nuclear Instruments and Methods in Physics Research Section B: Beam Interactions with Materials and Atoms **268**, 1818 (2010). Version code available from http://www.srim.org, 2013.
[11]M. H. Wong, K. Sasaki, A. Kuramata, S. Yamakoshi, and M. Higashiwaki, Appl. Phys. Lett. **106**, 032105 (2015).
[12]A. K. Rajapitamahuni, A. K. Manjeshwar, A. Kumar, A. Datta, P. Ranga, L. R. Thoutam, S. Krishnamoorthy, U. Singisetti, and B. Jalan, ACS Nano **16**, 8812 (2022).
[13]A. Azarov, C. Bazioti, V. Venkatachalapathy, P. Vajeeston, E. Monakhov, and A. Kuznetsov, Phys. Rev. Lett. **128**, 015704 (2022).
[14]I. Cora, F. Mezzadri, F. Boschi, M. Bosi, M. Čaplovičová, G. Calestani, I. Dódony, B. Pécz, and R. Fornari, CrystEngComm **19**, 1509 (2017).
[15]C. S. Chang, N. Tanen, V. Protasenko, T. J. Asel, S. Mou, H. G. Xing, D. Jena, and D. A. Muller, APL Mater. **9**, 051119 (2021).
[16]A. Debelle and A. Declémy, Nucl. Instrum. Methods Phys. Res. Sect. B: Beam Interact. Mater. Atoms **268**, 1460 (2010).
[17]V. Trushin, A. Nikolskaya, D. Korolev, A. Mikhaylov, A. Belov, E. Pitirimova, D. Pavlov, and D. Tetelbaum, Mater. Lett. **319**, 132248 (2022).
[18]M. J. Tadjer, C. Fares, N. A. Mahadik, J. A. Freitas, D. Smith, R. Sharma, M. E. Law, F. Ren, S. J. Pearton, and A. Kuramata, ECS J. Solid State Sci. Technol. **8**, Q3133 (2019).
[19]K. Tetzner, A. Thies, E. Bahat Treidel, F. Brunner, G. Wagner, and J. Würfl, Appl. Phys. Lett. **113**, 172104 (2018).